Springer Ser Chem Sens Biosens (2006) 4: 45–67
DOI 10.1007/5346_014

Published online: 8 July 2006

Surface Plasmon Resonance (SPR) Sensors

Jiří Homola (✉) · Marek Piliarik

Institute of Radio Engineering and Electronics, Prague, Czech Republic
homola@ure.cas.cz

Keywords Affinity biosensor · Guided mode · Optical sensor · Spectroscopy of guided modes · Surface plasmon resonance sensor

1 Introduction

In Chap. 1 by J. Homola of this volume [1] surface plasmons were introduced as modes of dielectric/metal planar waveguides and their properties were established. It was demonstrated that the propagation constant of a surface plasmon is sensitive to variations in the refractive index at the surface of a metal film supporting the surface plasmon. In this chapter, it is shown how this phenomenon can be used to create a sensing device. The concept of optical sensors based on surface plasmons, commonly referred as to surface plasmon resonance (SPR) sensors, is described and the main approaches to SPR sensing are presented. In addition, the concept of affinity biosensors is introduced and the main performance characteristics of SPR biosensors are defined.

2 Surface Plasmon Resonance (SPR) Sensors

An optical sensor is a sensing device which, by optical means, converts the quantity being measured (measurand) to another quantity (output) which is typically encoded into one of the characteristics of a light wave. In SPR sensors, a surface plasmon is excited at the interface between a metal film and a dielectric medium (superstrate), changes in the refractive index of which are to be measured. A change in the refractive index of the superstrate produces a change in the propagation constant of the surface plasmon. This change alters the coupling condition between a light wave and the surface plasmon, which can be observed as a change in one of the characteristics of the optical wave interacting with the surface plasmon [2]. Based on which characteristic of the light wave interacting with the surface plasmon is measured, SPR sensors can be classified as SPR sensors with angular, wavelength, intensity, phase, or polarization modulation (Fig. 1).

In *SPR sensors with angular modulation* a monochromatic light wave excites a surface plasmon. The strength of coupling between the incident wave and the surface plasmon is observed at multiple angles of incidence of the light wave and the angle of incidence yielding the strongest coupling is measured and used as a sensor output (Fig. 2, upper plot) [3]. The sensor output can be calibrated to refractive index. In *SPR sensors with wavelength modulation*, a surface plasmon is excited by a collimated light wave containing multiple wavelengths. The angle at which the light wave is incident onto the metal film is kept constant. The strength of coupling between the incident wave and the surface plasmon is observed at multiple wavelengths and the wavelength yielding the strongest coupling is measured and used as a sensor output (Fig. 2, lower plot) [4]. *SPR sensors with intensity modulation* are

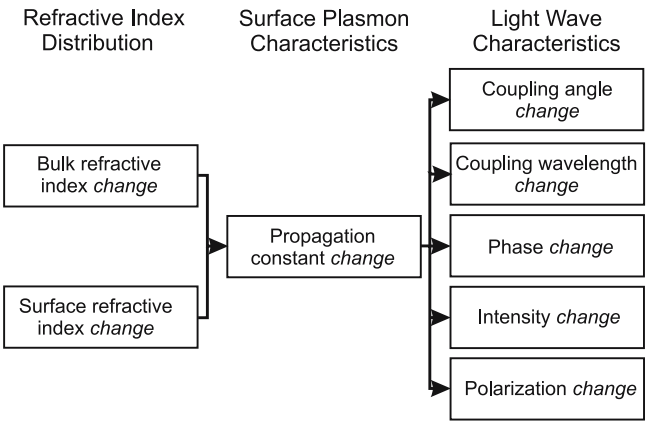

Fig. 1 Concept of surface plasmon resonance sensors

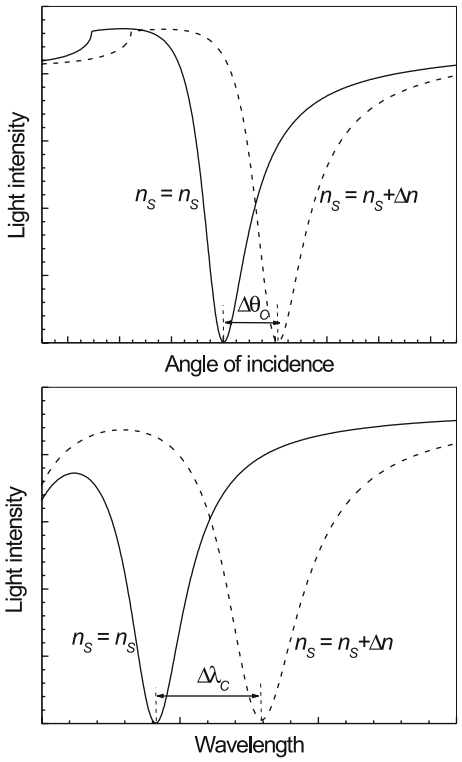

Fig. 2 Intensity of light wave interacting with a surface plasmon as a function of angle of incidence (*upper plot*) and wavelength (*lower plot*) for two different refractive indices of superstrate

based on measuring the strength of the coupling between the incident light wave and a surface plasmon at a single angle of incidence and wavelength and the intensity of light wave serves as a sensor output [5]. In *SPR sensors with phase modulation* the shift in phase of the light wave interacting with the SP is measured at a single angle of incidence and wavelength of the light wave and used as a sensor output [6]. In *SPR sensors with polarization modulation*, changes in the polarization of the light wave interacting with a surface plasmon are measured [7].

SPR sensors are either direct or indirect. In direct SPR sensors, the measurand (typically refractive index) modulates characteristics of the light directly. In indirect SPR sensors, the measurand modulates an intermediate quantity which then modulates the light characteristics. SPR affinity biosensors are a typical example of indirect SPR sensors.

3
Surface Plasmon Resonance Affinity Biosensors

SPR affinity biosensors are SPR sensing devices incorporating biorecognition elements (e.g., antibodies) that recognize and are able to interact with a selected analyte. The biorecognition elements are immobilized on the surface of a metal film supporting a surface plasmon. When a solution containing analyte molecules is brought into contact with the SPR sensor, analyte molecules in solution bind to the molecular recognition elements, producing an increase in the refractive index at the sensor surface. This change gives rise to a change in the propagation constant of the surface plasmon (Fig. 3). The change in the propagation constant is determined by measuring a change in one of the characteristics of the light wave interacting with the surface plasmon (Fig. 1) [2].

The amount of the refractive index change Δn_b induced by the analyte molecules binding to the biorecognition elements depends on the volume refractive index increment $(\mathrm{d}n/\mathrm{d}c)_{vol}$ and can be expressed as:

$$\Delta n_b = \left(\frac{\mathrm{d}n}{\mathrm{d}c}\right)_{vol} \Delta c_b \,, \tag{1}$$

where Δc_b is the concentration of bound analyte expressed in mass/volume. The value of the refractive index increment depends on the structure of the analyte molecules and varies from 0.1 to 0.3 mL g^{-1} [8, 9]. If the binding occurs within a thin layer at the sensor surface of thickness h the refractive index change can be rewritten as:

$$\Delta n_b = \left(\frac{\mathrm{d}n}{\mathrm{d}c}\right)_{vol} \frac{\Delta \Gamma}{h} \,, \tag{2}$$

where Γ denotes the surface concentration in mass/area [10].

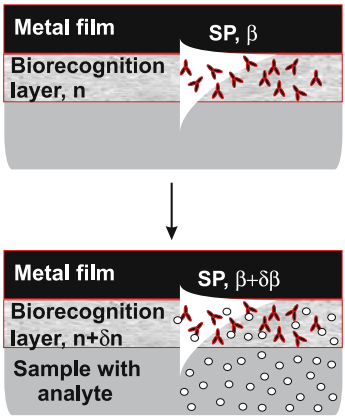

Fig. 3 Principle of surface plasmon resonance affinity biosensor

4 Main Performance Characteristics of SPR Sensors

In direct (refractometric) SPR sensors, refractive index (measurand) directly modulates characteristics of the light wave such as the coupling angle or wavelength, intensity, phase, and polarization (sensor output) (Fig. 4, upper diagram). In SPR affinity biosensors, the measurand is usually a concentration of a chemical or biological analyte, which through the binding of analyte to a biorecognition element is converted into a refractive index change at the sensor surface, which then modulates characteristics of the light wave (sensor output) (Fig. 4, lower diagram).

The sensor response to a given value of the measurand can be predicted by the sensor transfer function F, $Y = F(X)$ determined from a theoretical sensor model or a sensor calibration. However, the value of the measurand determined by the sensor X_{measured} differs from the true value of the measurand X_{true}:

$$X_{\text{measured}} = X_{\text{true}} + e\,, \tag{3}$$

by the measurement error e. There are various sources of error. Random errors are statistical fluctuations (in either direction) in the measured data due to the precision limitations of the sensor system. Random errors are not eliminated by calibration. Systematic errors, by contrast, are reproducible inaccuracies that are consistently in the same direction. Systematic errors are reduced by calibration to the uncertainty level of the calibration system. The uncertainty of a calibration depends primarily on the accuracy of the reference(s) and stability of the test environment.

The main characteristics describing the performance of SPR (bio)sensors include sensitivity, linearity, resolution, accuracy, reproducibility, dynamic range, limit of detection, and limit of quantification.

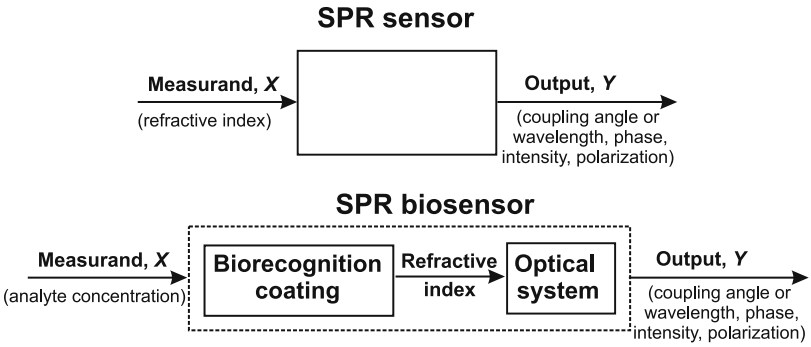

Fig. 4 Direct and indirect SPR sensors: measurand and sensor output

Sensor *sensitivity* is the ratio of the change in sensor output to the change in the measurand (slope of the calibration curve):

$$S = \frac{\partial Y}{\partial X} . \tag{4}$$

Refractometric sensitivity describes the sensitivity of the SPR sensor to refractive index n and can be written as:

$$S_{\mathrm{RI}} = \frac{\partial Y}{\partial n} . \tag{5}$$

Sensitivity of an SPR biosensor to a concentration of analyte c can be written as:

$$S_{\mathrm{c}} = \frac{\partial Y}{\partial c} . \tag{6}$$

Sensitivity of SPR sensors will be discussed in detail in Sect. 4.1.

Sensor *linearity* may concern primary measurand (concentration of analyte) or refractive index and defines the extent to which the relationship between the measurand and sensor output is linear over the working range. Linearity is usually specified in terms of the maximum deviation from a linear transfer function over the specified dynamic range. In general, sensors with linear transfer functions are desirable as they require fewer calibration points to produce an accurate sensor calibration. However, response of SPR biosensors is usually a non-linear function of the analyte concentration and therefore calibration needs to be carefully considered.

The *resolution* of a sensor is the smallest change in measurand which produces a detectable change in the sensor output. In SPR sensors, the term resolution usually refers to a bulk refractive index resolution. In SPR biosensors, an equivalent of this term is the limit of detection described below. Resolution of SPR sensors will be discussed in detail in Sect. 4.2.

Sensor *accuracy* describes the closeness of agreement between a measured value and a true value of the measurand (concentration of analyte or refractive index). Sensor accuracy is usually expressed in absolute terms or as a percentage of the error/output ratio.

Reproducibility is the ability of the sensor to provide the same output when measuring the same value of the measurand (concentration of analyte or refractive index) under the same operating conditions over a period of time. The reproducibility is typically expressed as the percentage of full range.

The (*dynamic*) *range* describes the span of the values of the measurand that can be measured by the sensor. In refractometric SPR sensors the dynamic range usually describes a range of values of the refractive index of the sample that can be measured with a specified accuracy. Dynamic range of SPR biosensors defines the range of concentrations of an analyte which can be measured with specified accuracy and extends from the lowest concen-

tration at which a quantitative measurement can be done, i.e., the limit of quantification.

An important characteristic describing the ability of a biosensor to detect an analyte is the *limit of detection* (LOD). LOD, as defined by the International Union of Pure and Applied Chemistry, is the concentration of analyte c_L derived from the smallest measure Y_L that can be detected with reasonable certainty. The value of Y_{LOD} is given by the equation:

$$Y_{LOD} = Y_{blank} + m\sigma_{blank}\,, \tag{7}$$

where Y_{blank} is the mean of the blank (sample with no analyte) measures, σ_{blank} is the standard deviation of the blank measures, and m is a numerical factor chosen according to the confidence level desired (typically 2 or 3) [11]. As $c_{blank} = 0$, the LOD concentration c_{LOD} can be expressed as:

$$c_{LOD} = \frac{1}{S_c(c=0)} m\sigma_{blank}\,, \tag{8}$$

where S_c denotes the sensor sensitivity to analyte concentration. It should be noted that this definition of LOD inherently recognizes only the false positives, which in effect makes the probability of a false negative equal to 50% [11]. Therefore, another approach to the definition of LOD can be found in the literature, employing two independent values (each equal to 0.05 or 0.01) for the probability of the false positives and negatives [12].

As the LOD defined by Eq. 8 defines the concentration at which one can decide whether the analyte is present, rather than quantifying the analyte concentration, another performance characteristic – the *limit of quantification* (LOQ) – is sometimes used [11]. Analyte quantification is generally accepted to begin at a concentration equal to 10 standard deviations of the blank. Thus, the LOQ concentration c_{LOQ}, can be expressed as:

$$c_{LOQ} = \frac{10}{S_c(c=0)} \sigma_{blank}\,. \tag{9}$$

4.1 Sensitivity

The sensitivity of an SPR biosensor can be decomposed into two contributions:

$$S_c = \frac{\partial Y}{\partial c} = \frac{\partial Y}{\partial n_b} \frac{\mathrm{d}n_b(c)}{\mathrm{d}c} = S_{RI} S_{nc}\,, \tag{10}$$

where S_{RI} denotes the sensitivity of the output to a refractive index profile change and S_{nc} is derived from the refractive index change (n_b) caused by the binding of analyte (concentration c) to biorecognition elements. The sensitivity of an SPR sensor to a refractive index S_{RI} can be also broken down into two

contributions:

$$S_{\mathrm{RI}} = \frac{\delta Y}{\delta n_{\mathrm{ef}}} \frac{\delta n_{\mathrm{ef}}}{\delta n_{\mathrm{b}}} = S_{\mathrm{RI1}} S_{\mathrm{RI2}} \,. \tag{11}$$

The first term S_{RI1} depends on the method of excitation of surface plasmons and the modulation approach used in the SPR sensor and is hereafter referred as to the instrumental contribution. S_{RI2} describes the sensitivity of the effective index of a surface plasmon to refractive index and is independent of the modulation method and the method of excitation of surface plasmons. The sensitivity of surface plasmon to refractive index S_{RI2} depends on the profile of the refractive index n_{b} and has been analyzed in Chap. 1 of this volume [1] for the two main types of refractive index changes – surface refractive index change and bulk refractive index change.

In the following section, sensitivity of the sensor output to effective index of a surface plasmon is analyzed for selected sensor configurations, and the merit of different SPR sensor configurations in terms of bulk refractive index sensitivity is evaluated.

4.1.1 Sensitivity of SPR Sensors with Angular Modulation

In SPR sensors with angular modulation, the sensor output is the coupling angle θ_{r} and therefore the instrumental contribution to sensor sensitivity S_{RI1} is equal to $\delta\theta_{\mathrm{r}}/\delta n_{\mathrm{ef}}$. After a straightforward manipulation, differentiation of the coupling conditions for the prism coupler (see Chap. 1 of this volume [1]) in n_{ef} and θ (θ_i for the grating coupler, the angle of incidence is given in a medium with a refractive index $n_i = 1$), yields:

$$\left(\frac{\delta\theta_{\mathrm{r}}}{\delta n_{\mathrm{ef}}}\right)_{\mathrm{prism}} = \frac{1}{n_{\mathrm{p}} \cos\theta_{\mathrm{r}}} = \frac{1}{\sqrt{n_{\mathrm{p}}^2 - n_{\mathrm{ef}}^2}} \,, \tag{12}$$

where n_{p} is the refractive index of the prism. Similarly, by differentiating the coupling condition for the grating coupler (see Chap. 1 in this volume [1]), one can obtain:

$$\left(\frac{\delta\theta_{\mathrm{r}}}{\delta n_{\mathrm{ef}}}\right)_{\mathrm{grating}} = \frac{\mathrm{sgn}(m)}{\cos\theta_{\mathrm{r}}} = \frac{\mathrm{sgn}(m)}{\sqrt{1 - \left(n_{\mathrm{ef}} - \frac{|m|\lambda}{\Lambda}\right)^2}} \,, \tag{13}$$

where m denotes the order of diffraction. Equation 13 suggests that $\left(\delta\theta_{\mathrm{r}}/\delta n_{\mathrm{ef}}\right)_{\mathrm{grating}}$ is positive for positive diffraction orders and negative for negative diffraction orders (resonant angle decreases with n_{ef} increase). An increase in the diffraction order can be compensated for by a decrease in the grating period Λ. Figure 5 depicts the wavelength dependence of $\delta\theta_{\mathrm{r}}/\delta n_{\mathrm{ef}}$ for model prism- and grating-based SPR sensors.

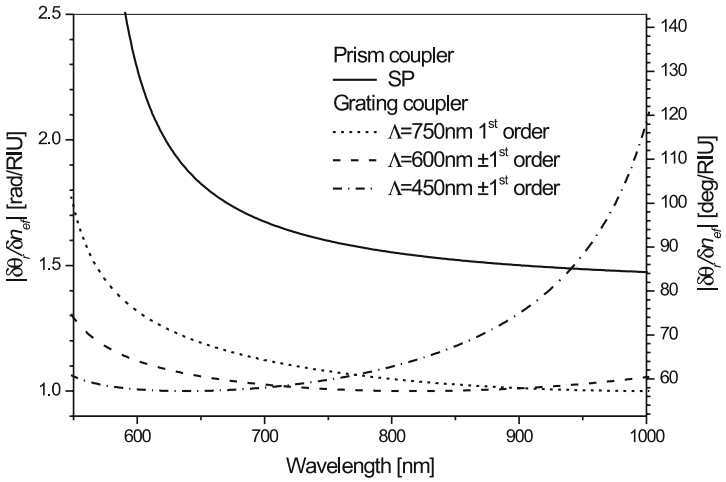

Fig. 5 Instrumental contribution to sensitivity $\delta\theta_r/\delta n_{ef}$ as a function of wavelength for SPR sensors with angular modulation and prism coupler or grating coupler and three different grating periods. Prism-based sensor configuration: BK7 glass prism, gold film, and a non-dispersive dielectric (refractive index 1.32). Grating-based sensor configuration: a non-dispersive dielectric (refractive index 1.32) and gold grating

As follows from Fig. 5, the sensitivity $\left(\delta\theta_r/\delta n_{ef}\right)_{prism}$ increases with a decreasing wavelength following the wavelength dependence of the effective index of the surface plasmon and the coupling angle (see Chap. 1 of this volume [1]). The rapid increase of $\left(\delta\theta_r/\delta n_{ef}\right)_{prism}$ at short wavelengths is associated with the effective index of a surface plasmon n_{ef} approaching the refractive index of the prism n_p (and angle of incidence approaching 90 deg). The instrumental contribution to sensitivity $\left(\delta\theta_r/\delta n_{ef}\right)_{grating}$ exhibits a minimum that corresponds to the normal incidence ($\lambda = \Lambda n_{ef}$) and increases both towards long and short wavelengths.

For SPR sensors with angular modulation using coupled surface plasmons on a thin metal film (instead of conventional surface plasmons on a metal–dielectric interface), the instrumental contribution to sensitivity $\delta\theta_r/\delta n_{ef}$ can also be calculated from Eqs. 12 and 13.

As follows from Eq. 12, the instrumental contribution $\left(\delta\theta_r/\delta n_{ef}\right)_{prism}$ is determined by the difference between the refractive index of the prism and effective index of the surface plasmon. Therefore, the highest sensitivity can be obtained using an antisymmetric surface plasmon (which, however, exists only within a range of wavelengths at which its effective index is smaller than the refractive index of prism) (Fig. 6). SPR sensors employing a symmetric surface plasmon are less sensitive than those using conventional plasmon at a metal–dielectric interface (Fig. 6). The sensitivity

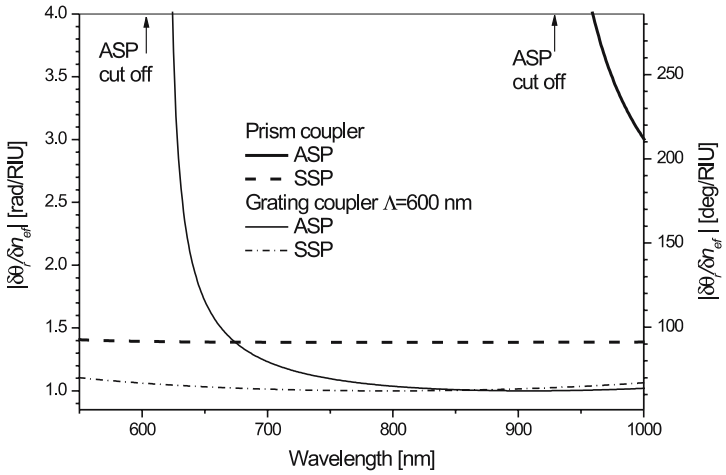

Fig. 6 Instrumental contribution to sensitivity $\delta\theta_r/\delta n_{ef}$ as a function of wavelength for an SPR sensor with angular modulation which employs symmetric (SSP) and antisymmetric (ASP) surface plasmons excited on a thin gold film using prism or grating coupler. Prism-based sensor configuration: BK7 glass prism, buffer layer (refractive index 1.32), gold film (thickness 20 nm), and a non-dispersive dielectric (refractive index 1.32).Grating-based sensor configuration: a non-dispersive dielectric (refractive index 1.32) and grating (grating period 600 nm) supporting a gold film (thickness 20 nm) and a buffer layer (refractive index 1.32)

$\left(\delta\theta_r/\delta n_{ef}\right)_{grating}$ of grating-based SPR sensors using symmetric and antisymmetric surface plasmons follows basically the same trend, however, the cut-off for the antisymmetric mode $\left(n_{ef} = (\lambda m/\Lambda + 1)\right)$ is shifted to shorter wavelengths.

Once the instrumental contribution to sensitivity $\delta\theta_r/\delta n_{ef}$ of an SPR sensor has been determined, the sensitivity to refractive index can be calculated as follows:

$$S_{RI} = \left|\frac{\delta\theta_r}{\delta n_{ef}}\right| \frac{\delta n_{ef}}{\delta n}, \tag{14}$$

where the term $\delta n_{ef}/\delta n$ describes the sensitivity of the effective index of a surface plasmon to refractive index and depends on the details of the distribution of the refractive index change. In the following section we calculate the sensor sensitivity to bulk refractive index change to illustrate this process and to provide a practical means for evaluation of the sensitivity of various configurations of SPR sensors.

The sensitivity of angular modulation-based SPR sensors to bulk refractive index (herein denoted as $\left(S_\theta\right)_{prism}$ and $\left(S_\theta\right)_{grating}$ for SPR sensors using prism and grating couplers, respectively) can be derived from Eqs. 12 and 13, and the equation for $\delta n_{ef}/\delta n$ obtained using the perturbation theory (Eq. 58

in Chap. 1 of this volume [1]) [13]:

$$\left(S_\theta\right)_{\text{prism}} = \frac{\varepsilon'_m\sqrt{-\varepsilon'_m}}{\left(\varepsilon'_m + n^2\right)\sqrt{\varepsilon'_m\left(n^2 - n_{\text{p}}^2\right) - n^2 n_{\text{p}}^2}}, \tag{15}$$

$$\left(S_\theta\right)_{\text{grating}} = \frac{\varepsilon'_m\sqrt{-\varepsilon'_m}}{\left(\varepsilon'_m + n^2\right)\sqrt{\left(1 - \frac{m^2\lambda^2}{\Lambda^2}\right)\left(n^2 + \varepsilon'_m\right) - n^2\varepsilon'_m + 2n\frac{|m|\lambda}{\Lambda}\sqrt{\varepsilon'_m\left(n^2 + \varepsilon'_m\right)}}}, \tag{16}$$

where ε'_m is the real part of the permittivity of metal. Bulk refractive index sensitivities of model SPR sensors with angular modulation and prism and grating coupler were calculated using (Eq. 15) and (Eq. 16) and are shown in Fig. 7. As the sensitivity of the effective index of the surface plasmon to bulk refractive index decreases slowly with an increasing wavelength, the behavior of the bulk refractive index sensitivity basically follows the instrumental contribution $\delta\theta_{\text{r}}/\delta n_{\text{ef}}$. The bulk refractive index sensitivity of SPR sensors using symmetric or antisymmetric surface plasmons is also dominated by the instrumental contribution $\delta\theta_{\text{r}}/\delta n_{\text{ef}}$ (Fig. 8).

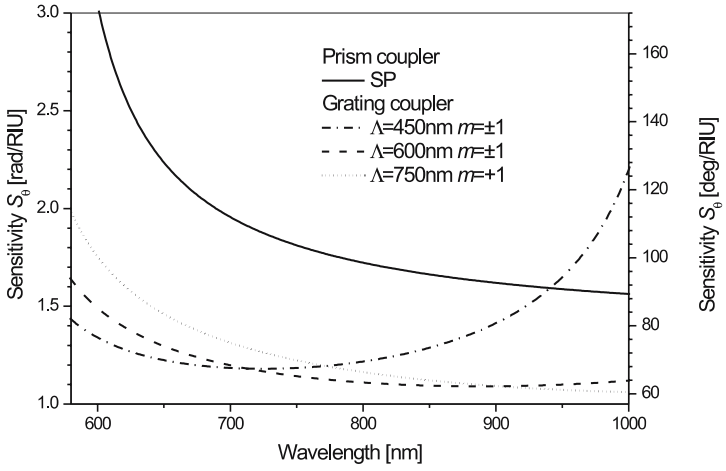

Fig. 7 Bulk refractive index sensitivity as a function of wavelength for SPR sensors with angular modulation and prism coupler or grating coupler and three different grating periods. Prism-based sensor configuration: BK7 glass prism, gold film, and a non-dispersive dielectric (refractive index1.32). Grating-based sensor configuration: a non-dispersive dielectric (refractive index 1.32) and gold grating

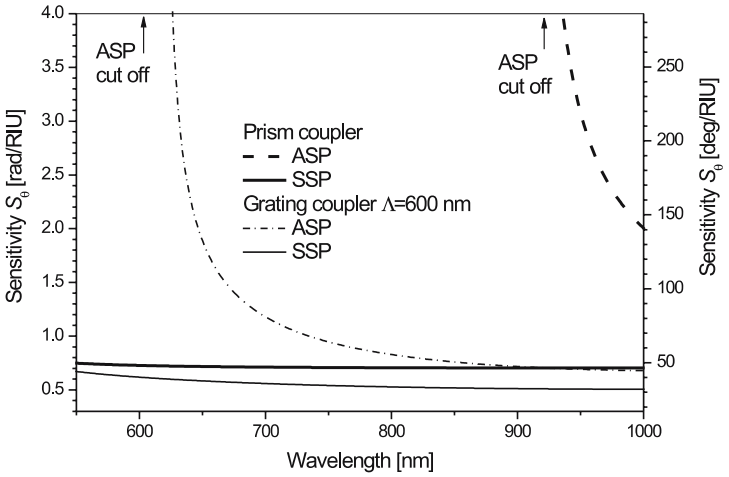

Fig. 8 Bulk refractive index sensitivity as a function of wavelength for an SPR sensor with angular modulation which employs symmetric (SSP) and antisymmetric (ASP) surface plasmons excited on a thin gold film using prism or grating coupler. Prism-based sensor configuration: BK7 glass prism, buffer layer (refractive index 1.32), gold film (thickness 20 nm), and a non-dispersive dielectric (refractive index 1.32). Grating-based sensor configuration: a non-dispersive dielectric (refractive index 1.32) and grating (grating period 600 nm) supporting a gold film (thickness 20 nm) and a buffer layer (refractive index 1.32)

4.1.2 Sensitivity of SPR Sensors with Wavelength Modulation

In SPR sensors with angular modulation, the sensor output is the coupling wavelength λ_r and therefore the instrumental contribution to sensor sensitivity S_{RI1} is equal to $\delta\lambda_r/\delta n_{ef}$. By differentiating the coupling conditions for the prism, grating, and waveguide coupler (see Chap. 1 of this volume [1]) in n_{ef} and λ, we obtain:

$$\left(\frac{\delta\lambda_r}{\delta n_{ef}}\right)_{prism} = \frac{1}{\frac{dn_p}{d\lambda}\frac{n_{ef}}{n_p} - \frac{dn_{ef}}{d\lambda}}, \tag{17}$$

$$\left(\frac{\delta\lambda_r}{\delta n_{ef}}\right)_{grating} = \frac{1}{\frac{|m|}{\Lambda} - \frac{dn_{ef}}{d\lambda}}, \tag{18}$$

$$\left(\frac{\delta\lambda_r}{\delta n_{ef}}\right)_{waveguide} = \frac{1}{\frac{dn_{wg}}{d\lambda} - \frac{dn_{ef}}{d\lambda}}, \tag{19}$$

where the derivatives $dn_{ef}/d\lambda$, $dn_p/d\lambda$ and $dn_{wg}/d\lambda$ describe the dispersion of the effective index of a surface plasmon, dispersion of the coupling prism, and chromatic dispersion of the waveguide, respectively. The dispersion of

glasses constituting prism couplers is usually much smaller than the dispersion of surface plasmons on a metal–dielectric interface. For the wavelengths and typical materials used in waveguide-based SPR sensors, the chromatic dispersion $\mathrm{d}n_{\mathrm{wg}}/\mathrm{d}\lambda$ is to a large extent determined by the material dispersion of the waveguide. The wavelength dependence of the instrumental contribution to sensitivity $\delta\lambda_{\mathrm{r}}/\delta n_{\mathrm{ef}}$ for model prism and grating-based SPR sensors, calculated using Eqs. 17 and 18, is shown in Fig. 9.

The instrumental contribution to sensitivity of SPR sensors using prism couplers $\left(\delta\lambda_{\mathrm{r}}/\delta n_{\mathrm{ef}}\right)_{\mathrm{prism}}$ is primarily determined by the second term in the denominator of Eq. 17 $\mathrm{d}n_{\mathrm{ef}}/\mathrm{d}\lambda$ and therefore $\left(\delta\lambda_{\mathrm{r}}/\delta n_{\mathrm{ef}}\right)_{\mathrm{prism}}$ increases with increasing wavelength. The instrumental contribution to sensitivity $\left(\delta\lambda_{\mathrm{r}}/\delta n_{\mathrm{ef}}\right)_{\mathrm{grating}}$ increases with an increasing wavelength and levels off as the term m/Λ dominates over $\mathrm{d}n_{\mathrm{ef}}/\mathrm{d}\lambda$. The instrumental contribution to sensitivity of SPR sensors with prism coupler $\left(\delta\lambda_{\mathrm{r}}/\delta n_{\mathrm{ef}}\right)_{\mathrm{prism}}$ is typically larger by an order of magnitude than that for a grating coupler $\left(\delta\lambda_{\mathrm{r}}/\delta n_{\mathrm{ef}}\right)_{\mathrm{grating}}$.

For SPR sensors with wavelength modulation using coupled surface plasmons on a thin metal film (instead of conventional surface plasmons on a metal–dielectric interface), the instrumental contribution to sensitivity $\delta\lambda_{\mathrm{r}}/\delta n_{\mathrm{ef}}$ can be also calculated from Eqs. 17 and 18 (Fig. 10). The wavelength dependence of the instrumental contribution to sensitivity $\delta\lambda_{\mathrm{r}}/\delta n_{\mathrm{ef}}$ for model prism and grating-based SPR sensors employing symmetric and antisymmet-

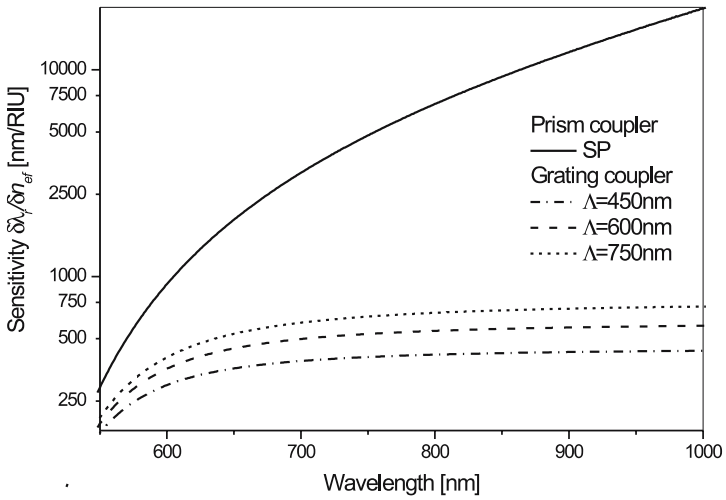

Fig. 9 Instrumental contribution to sensitivity $\delta\lambda_{\mathrm{r}}/\delta n_{\mathrm{ef}}$ as a function of wavelength for SPR sensors with wavelength modulation and prism coupler or grating coupler and three different grating periods. Prism-based sensor configuration: BK7 glass prism, gold film, and a non-dispersive dielectric (refractive index 1.32). Grating-based sensor configuration: a non-dispersive dielectric (refractive index 1.32) and gold grating

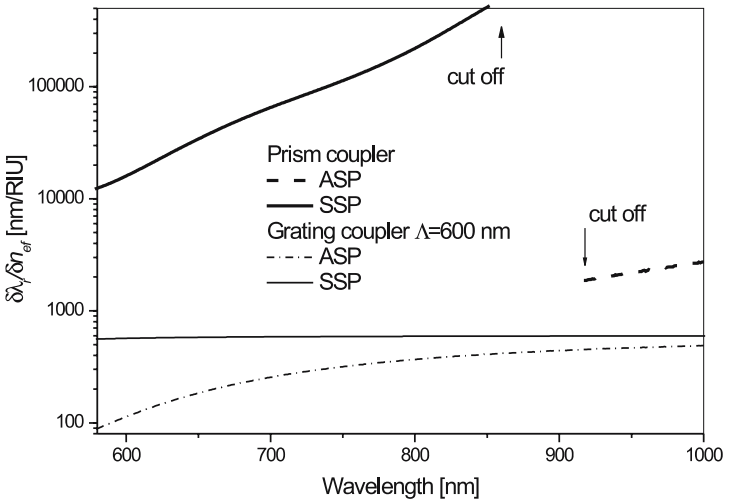

Fig. 10 Instrumental contribution to sensitivity $\delta\lambda_r/\delta n_{ef}$ as a function of wavelength for an SPR sensor with wavelength modulation which employs symmetric (SSP) and antisymmetric (ASP) surface plasmons excited on a thin gold film using prism or grating coupler. Prism-based sensor configuration: BK7 glass prism, buffer layer (refractive index 1.32), gold film (thickness 20 nm), and a non-dispersive dielectric (refractive index 1.32). Grating-based sensor configuration: a non-dispersive dielectric (refractive index 1.32) and grating (grating period 600 nm) supporting a gold film (thickness 20 nm) and a buffer layer (refractive index 1.32)

ric surface plasmons, calculated using Eqs. 17 and 18, is shown in Fig. 10. The instrumental contribution to sensitivity $\left(\delta\lambda_r/\delta n_{ef}\right)_{prism}$ for the symmetric surface plasmon increases until the denominator in Eq. 17 reaches zero [14] and is larger by an order of magnitude than that for the conventional surface plasmon on a metal–dielectric interface, or for the antisymmetric surface plasmon. The instrumental contribution to sensitivity of SPR sensors using grating couplers $\left(\delta\lambda_r/\delta n_{ef}\right)_{grating}$ and symmetric or antisymmetric surface plasmon increases with increasing wavelength and is significantly smaller than $\left(\delta\lambda_r/\delta n_{ef}\right)_{prism}$ and comparable with $\left(\delta\lambda_r/\delta n_{ef}\right)_{grating}$ values obtained using conventional surface plasmons on gold–dielectric interface.

Once the instrumental contribution to sensitivity $\delta\lambda_r/\delta n_{ef}$ of an SPR sensor has been determined, the sensitivity to refractive index can be calculated as follows:

$$S_{RI} = \frac{\delta\lambda_r}{\delta n_{ef}} \frac{\delta n_{ef}}{\delta n}, \tag{20}$$

where the term $\delta n_{ef}/\delta n$ describes the sensitivity of the effective index of a surface plasmon to refractive index and depends on the details of the distribution of the refractive index change. The spectral sensitivity of SPR sensors based on prism and grating couplers and wavelength modulation for conven-

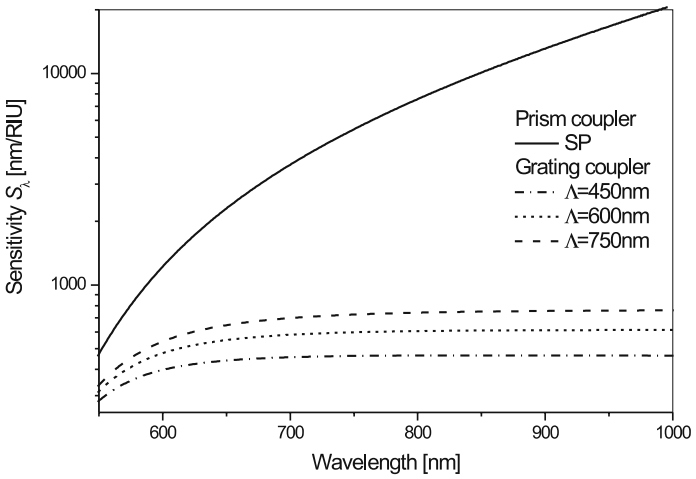

Fig. 11 Bulk refractive index sensitivity as a function of wavelength for SPR sensors with wavelength modulation and prism coupler or grating coupler and three different grating periods. Prism-based sensor configuration: BK7 glass prism, gold film, and a non-dispersive dielectric (refractive index 1.32). Grating-based sensor configuration: a non-dispersive dielectric (refractive index 1.32) and gold grating

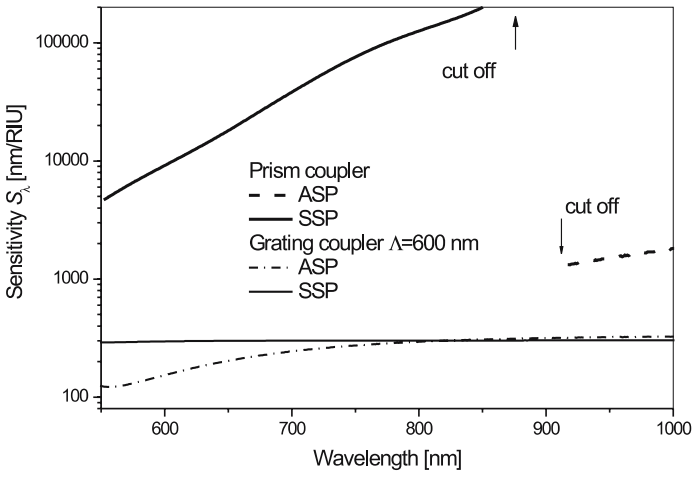

Fig. 12 Bulk refractive index sensitivity as a function of wavelength for SPR sensors with wavelength modulation employing symmetric (SSP) and antisymmetric (ASP) surface plasmons excited on a thin gold film using prism or grating coupler. Prism-based sensor configuration: BK7 glass prism, buffer layer (refractive index 1.32), gold film (thickness 20 nm), and a non-dispersive dielectric (refractive index 1.32). Grating-based sensor configuration: a non-dispersive dielectric (refractive index 1.32) and grating (grating period 600 nm) supporting a gold film (thickness 20 nm) and a buffer layer (refractive index 1.32)

tional surface plasmons on a gold–dielectric interface and coupled surface plasmons on a thin gold film is shown in Figs. 11 and 12.

Analytical expressions for sensitivity of SPR sensors with wavelength modulation can be derived from Eq. 20 using Eqs. 17 and 18 ($\delta n_{\mathrm{ef}}/\delta n$ is taken from Eq. 58 in Chap. 1 of this volume [1]) or directly from the coupling conditions [13]:

$$\left(S_\lambda\right)_{\mathrm{prism}} = \frac{\varepsilon_m'^2}{-\frac{n^3}{2}\frac{\mathrm{d}\varepsilon_m'}{\mathrm{d}\lambda} + \varepsilon_m'\left(n^2+\varepsilon_m'\right)\frac{n}{n_\mathrm{p}}\frac{\mathrm{d}n_\mathrm{p}}{\mathrm{d}\lambda}}\,, \tag{21}$$

$$\left(S_\lambda\right)_{\mathrm{grating}} = \frac{\varepsilon_m'^2}{-\frac{n^3}{2}\frac{\mathrm{d}\varepsilon_m'}{\mathrm{d}\lambda} + \frac{|m|}{\Lambda}\left(n^2+\varepsilon_m'\right)\sqrt{\varepsilon_m'\left(n^2+\varepsilon_m'\right)}}\,, \tag{22}$$

where $\mathrm{d}\varepsilon_m'/\mathrm{d}\lambda$ and $\mathrm{d}n_\mathrm{p}/\mathrm{d}\lambda$ represent the material dispersion of the metal and prism respectively.

4.1.3 Sensitivity of SPR Sensors with Intensity Modulation

In SPR sensors with intensity modulation, the sensor output is the intensity (which is proportional to reflectivity in prism or grating-based SPR sensor) and therefore the instrumental contribution to sensor sensitivity S_{RI1} can be written as $\delta R/\delta n_{\mathrm{ef}}$, where R denotes reflectivity. In order to derive analytical expressions for the instrumental contributions to sensor sensitivity, the reflectivity is assumes to follow the Lorentzian shape (Eq. 78 in Chap. 1 of this volume [1]):

$$R \doteq 1 - \frac{4\gamma_i\gamma_{\mathrm{rad}}}{\Delta_{\mathrm{ef}}^2 + (\gamma_i+\gamma_{\mathrm{rad}})^2}\,, \tag{23}$$

where γ_i and γ_{rad} denote the attenuation coefficients of surface plasmons due to the absorption and radiation, respectively [15] and:

$$\Delta_{\mathrm{ef}} = n_\mathrm{p}\sin\theta - n_{\mathrm{ef}}\,, \tag{24}$$

for prism coupler. Using Eq. 23, the sensitivity of reflectivity to effective refractive index can be expressed as follows:

$$\frac{\partial R}{\partial n_{\mathrm{ef}}} = \frac{-8\Delta_{\mathrm{ef}}\gamma_i\gamma_{\mathrm{rad}}}{\left[\Delta_{\mathrm{ef}}^2 + (\gamma_i+\gamma_{\mathrm{rad}})^2\right]^2}\,. \tag{25}$$

Yeatman et al. showed that the maximum slope of the reflectivity occurs when:

$$\Delta_{\mathrm{ef}} = \pm\frac{(\gamma_i+\gamma_{\mathrm{rad}})}{\sqrt{3}} \tag{26}$$

and that the maximum slope can be obtained when $\gamma_{\mathrm{rad}} = \gamma_i/2$ [16]. This condition reduces the depth of the resonant dip, but the decrease of its width

results in the increase of the reflectivity dependence slope. Under these conditions, the maximum instrumental contribution to sensitivity can be expressed as:

$$\frac{\delta R}{\delta n_{\mathrm{ef}}} = \left(\frac{\partial R}{\partial n_{\mathrm{ef}}}\right)_{\max} = \frac{2\sqrt{3}}{9\gamma_i}. \tag{27}$$

The wavelength dependence of the instrumental contribution to sensitivity $\delta R/\delta n_{\mathrm{ef}}$ for model prism-based SPR sensors calculated using Eq. 27 is shown in Fig. 13.

The bulk refractive index sensitivity can be calculated from the instrumental sensitivity in a similar fashion as in previous sections for the angular and wavelength modulation. The sensitivity to bulk refractive index can be expressed as:

$$S_{\mathrm{RI}} = \frac{\delta R}{\delta n_{\mathrm{ef}}}\frac{\delta n_{\mathrm{ef}}}{\delta n}. \tag{28}$$

The maximum sensitivity of intensity modulation-based SPR sensors to bulk refractive index $\left(S_{\mathrm{I}}\right)_{\max}$ can be derived from Eq. 28 (where $\delta n_{\mathrm{ef}}/\delta n$ is from

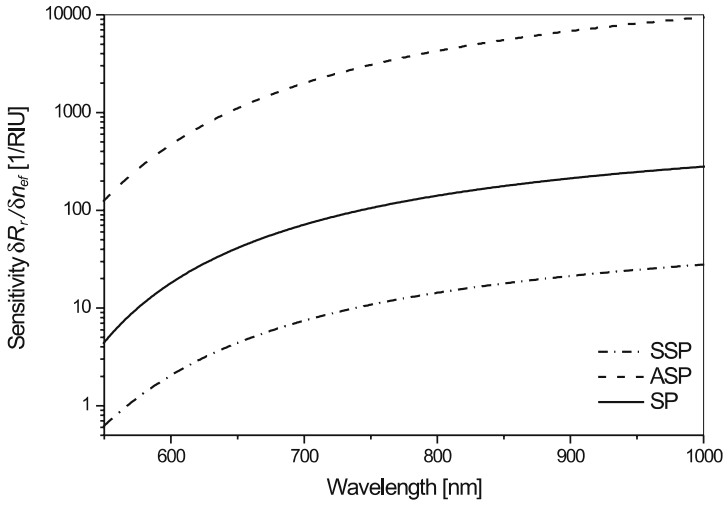

Fig. 13 Instrumental contribution to sensitivity $\delta R/\delta n_{\mathrm{ef}}$ as a function of wavelength for SPR sensors with intensity modulation and a prism coupler exciting a conventional surface plasmon (SP) at the interface of gold and a non-dispersive dielectric (refractive index 1.32) and coupled symmetric (SSP) and antisymmetric (ASP) surface plasmons on a thin gold film (thickness 20 nm) surrounded by two identical non-dispersive dielectrics (refractive index 1.32)

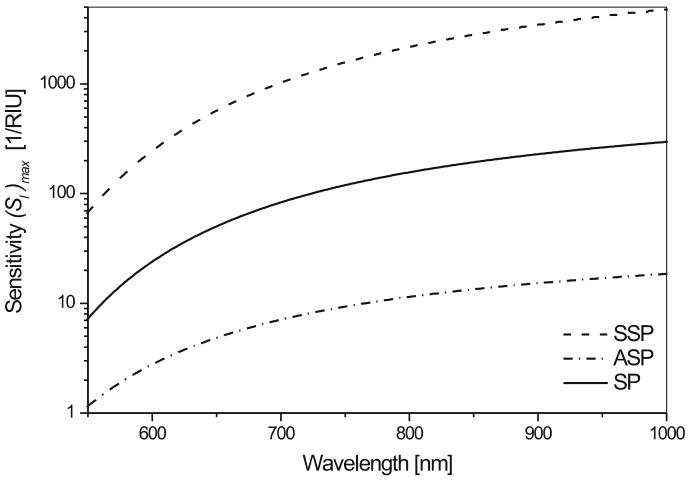

Fig. 14 The maximum bulk refractive index sensitivity as a function of wavelength for SPR sensors with intensity modulation and a prism coupler exciting a conventional surface plasmon (SP) at the interface of gold and a non-dispersive dielectric (refractive index 1.32) and coupled symmetric (SSP) and antisymmetric (ASP) surface plasmons on a thin gold film (thickness 20 nm) surrounded by two identical non-dispersive dielectrics (refractive index 1.32)

Eq. 58 in Chap. 1 of this volume [1]) as follows:

$$\left(S_{\mathrm{I}}\right)_{\max} = \frac{4\sqrt{3}}{9} \frac{\varepsilon_m'^2}{\varepsilon_m'' n^3}\,, \tag{29}$$

where ε_m' and ε_m'' are the real and imaginary part of the metal permittivity, respectively. Figure 14 shows the maximum sensitivity calculated using Eq. 28 for selected model SPR sensor configurations. As follows from Fig. 14, the bulk refractive index sensitivity of intensity-based sensors increases with increasing wavelength. This behavior is caused by the attenuation coefficient of surface plasmons, which decreases with increasing wavelength.

4.2 Resolution

Resolution of SPR sensors defines the smallest change in the bulk refractive index that produces a detectable change in the sensor output. The magnitude of sensor output change that can be detected depends on the level of uncertainty of the output, the output noise.

The noise of sensor output originates in the optical system and readout electronics of an SPR sensor instrument. Dominant sources of noise are fluctuations in the light intensity emitted by the light source, statistical properties

of light (shot noise), and noise in conversion of light intensity into photoelectrons by the detector and supporting circuitry.

The noise in the intensity of light emitted by the light source is proportional to the intensity and therefore its standard deviation σ can be given as $\sigma_L = \sigma_L^{rel} I$, where σ_L^{rel} is relative (intensity-independent) standard deviation and I denotes the measured light intensity.

The shot noise is associated with random arrival of photons on a detector and corresponding random production of photoelectrons. Conventional light sources produce photon flux that obeys Poisson statistics, which produces a shot noise σ_S directly proportional to the square root of the detected light intensity: $\sigma_S = \sigma_S^{rel}\sqrt{I}$, where σ_S^{rel} is relative (intensity-independent) standard deviation [17]. The detector noise consists of several contributions that originate mostly in temperature generated photoelectrons and the detector electronic circuitry, and its standard deviation σ_D is independent of the detected light intensity. The resulting noise of the measured light intensity σ_I is a statistical superimposition of all the noise components and can therefore be expressed as:

$$\sigma_I(I) = \sqrt{I^2\left(\sigma_L^{rel}\right)^2 + I\left(\sigma_S^{rel}\right)^2 + \sigma_D^2}\,. \tag{30}$$

In SPR sensors based on wavelength or angular modulations, multiple intensities corresponding to different wavelengths or angles of incidence are acquired. This results in series of wavelength or angular spectra in time ($I_1, I_2, I_3, \ldots, I_N$). These spectra are mathematically processed to generate the sensor output. In the first phase of data processing, the spectra are usually averaged (to reduce noise) and normalized (to eliminate effects of unequal angular or wavelength light distribution). The averaging either involves averaging of time series of intensity from the same detector (time averaging) or averaging of intensities from multiple detectors (e.g., of a 2D array) measured at a single time (spatial averaging). As in the time domain, all the noise contributions behave independently, the time averaging of N spectra reduces the noise of each intensity in the spectrum as follows:

$$\sigma_I^{tN} = \sqrt{I^2\frac{\left(\sigma_L^{rel}\right)^2}{N} + \frac{I\left(\sigma_S^{rel}\right)^2}{N} + \frac{\sigma_D^2}{N}} = \frac{\sigma_I}{\sqrt{N}}\,. \tag{31}$$

Spatial domain averaging can be applied when the sensor signal from N different detectors is averaged. In wavelength or angular modulation it is usually applied to spectra that are measured in several rows of a 2D detector [18, 19]. In sensors based on intensity modulation such as SPR imaging, the averaged area corresponds to one measuring channel [20–22]. In spatial averaging, the light fluctuations affect all the intensities measured by different detectors in the same way and therefore the light source noise is not reduced by the spatial

averaging:

$$\sigma_{\mathrm{I}}^{\mathrm{sN}} = \sqrt{I^2 \left(\sigma_{\mathrm{L}}^{\mathrm{rel}}\right)^2 + \frac{I\left(\sigma_{\mathrm{S}}^{\mathrm{rel}}\right)^2}{N} + \frac{\sigma_{\mathrm{D}}^2}{N}} > \frac{\sigma_{\mathrm{I}}}{\sqrt{N}} \,. \tag{32}$$

Therefore, especially in SPR sensors with intensity modulation, the light source noise can dominate over the shot noise and detector noise and needs to be reduced by other means.

The averaged and normalized spectra are translated into the sensor output by an appropriate data processing algorithm. Numerous methods for calculation of sensor output have been used in SPR sensors such as the centroid method [23, 24], polynomial fitting followed with the analytical calculation of the polynomial minimum [25, 26], and optimal linear data analysis [27]. As can be shown by a more general analysis, the noise in angular or wavelength spectra transforms to the noise in the sensor output in a similar fashion for the most common algorithms [28]. Therefore, we shall use the centroid method as a model data processing algorithm to illustrate the propagation of noise into the sensor output.

The centroid method uses a simple algorithm which finds the geometric center of the portion of the SPR dip under a certain threshold. Although the geometric center does not necessarily coincide with the minimum of the spectrum, as SPR sensing usually relies on relative measurements, the offset of the geometric center does not affect the final measurements. The centroid is calculated as follows:

$$Y_{\mathrm{C}} = \frac{\sum\limits_j x_j \left(I_{\mathrm{thresh}} - I_j\right)}{\sum\limits_j \left(I_{\mathrm{thresh}} - I_j\right)} \,, \tag{33}$$

where x_j represent the spectral positions of the contributing intensities I_j and I_{thresh} denotes the threshold value. If the noise of intensities detected by individual detectors can be treated as independent, the resulting standard deviation of calculated dip position (sensors output noise) σ_{so} can be derived from the noise of individual intensities $\sigma(I_j)$ as:

$$\sigma_{\mathrm{so}}^2 = \sum_{j=1}^{N} \left(\frac{\partial Y_{\mathrm{C}}}{\partial I_j}\right)^2 \sigma^2\left(I_j\right) \,, \tag{34}$$

where N is the number of involved intensities, and $\partial Y_{\mathrm{C}}/\partial I_j$ denotes the incremental contribution factors to the noise of dip position Y_{C} (sensor output) from each detector [29]. If we assume that the portion of the SPR dip used by the centroid algorithm follows the Lorentzian profile (see Chap. 1 in this volume [1]), that the optimum threshold level is at the half of the SPR dip

depth [29], and substitute Y_C from Eq. 33 in Eq. 34, we obtain:

$$\sigma_{so} \doteq \frac{1.75}{Nd} \sqrt{\sum_{j=1}^{N} (Y_C - x_j)^2 \sigma^2 \left(I_j\right)}, \tag{35}$$

where Y_C is the centroid position, N is the number of intensities below the threshold, and d is the depth of the dip (difference of intensities between the dip minimum and threshold). For the three types of noise discussed above: (a) the additive noise independent of the intensity, (b) the noise proportional to the square root of intensity (shot noise) and (c) the noise proportional to the intensity, Eq. 35 yields:

$$\sigma_{so} = K \frac{\sigma_{th}}{d} \cdot \frac{w}{\sqrt{N}}, \tag{36}$$

where σ_{th} is the intensity noise at threshold, d is the depth of the dip (difference of intensities between the dip minimum and threshold), w is the width of the dip (at the threshold) and $K = K_1 = 0.50$ for additive noise, $K = K_2 = 0.43$ for the shot noise, and $K = K_3 = 0.38$ for the noise proportional to the intensity. If the intensity noise is superimposition of the three types of noise with weights g_1, g_2, and g_3 ($g_1 + g_2 + g_3 = 1$), the coefficient K can be calculated as $K = \sqrt{g_1 K_1^2 + g_2 K_2^2 + g_3 K_3^2}$. This yields a refractive index uncertainty σ_{RI}:

$$\sigma_{RI} = \frac{\sigma_{so}}{S_{RI}} = K \frac{\sigma_{th}}{d\sqrt{N}} \cdot \frac{w}{S_{RI}}, \tag{37}$$

where S_{RI} denotes the bulk refractive index sensitivity of the sensor. The width of the SPR dip is directly correlated with its sensitivity and it can be shown that the ratio w/S_{RI} depends only weakly on the choice of coupler and modulation.

Equation 36 indicates that the sensor output noise is linearly dependent on the noise of measured signal and inverse linearly dependent on the depth of the SPR dip. If the number of measured intensities N is proportional to the investigated spectrum width, the sensor output noise depends on the square root of the width.

Using Eq. 37, the ultimate resolution of an SPR sensor can be predicted. Figure 15 shows theoretical resolutions calculated using Eq. 37 for SPR sensors employing three different types of detectors (a linear CCD detector, 2D CCD, and PDA detector). The following parameters were used for the simulations of the SPR sensor using a linear CCD detector: shot noise of 0.6% at the saturation level of the detector [29], and time averaging over 500 spectra (limited by typical readout and exposure times), which yields $\left(\sigma_{th}/d\right) = 4 \times 10^{-4}$ (threshold is set to half of the detector dynamical range). The following parameters were used for the SPR sensor using a 2D detec-

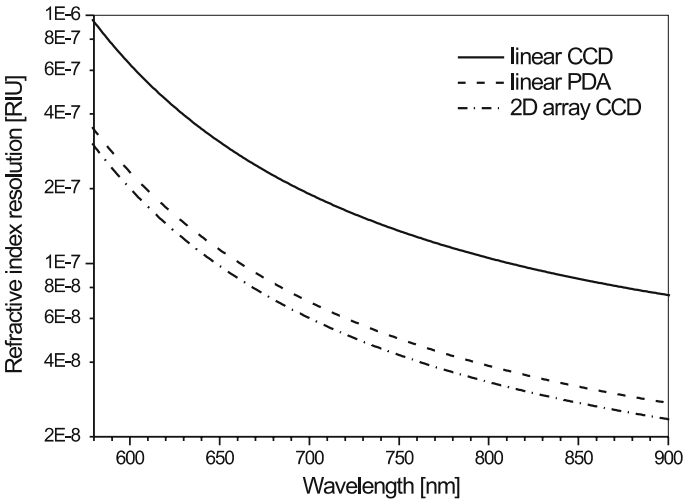

Fig. 15 Modeled resolution of SPR configuration with linear CCD, 2D CCD, and large area photodiode array (PDA) as a function of wavelength

tor: shot noise of 0.6%, spatial averaging over 100 detector lines [30], and time averaging over 50 spectra, which yields $\left(\sigma_{\text{th}}/\text{d}\right) = 1 \times 10^{-4}$ (threshold at half of the detector dynamical range). The following parameters were used for the simulations of the SPR sensor using a linear photodiode array (PDA) detector: the noise is dominantly additive ($g_1 = 0.8$, $g_2 = 0.2$, $K = 0.49$) and its SD relative to the threshold set to half of the detector dynamical range is 0.1% [29]. The time averaging over 50 spectra is supposed, yielding $\left(\sigma_{\text{th}}/\text{d}\right) = 1 \times 10^{-4}$. Furthermore, it is assumed that the width of the SPR dip covers 300 pixels ($N = 300$), which is close to the configuration analyzed in [29–31].

Figure 15 suggests that SPR sensors with large area detectors such as PDA or 2D array CCD can potentially achieve a better resolution compared to systems using linear CCD detectors. This comparison is related to the fact that more light is measured with large area detectors in the same period of time, which results in the reduction of the shot noise.

5 Summary

Surface plasmon resonance (SPR) sensors are optical sensing devices that take advantage of the sensitivity of a special type of electromagnetic field, a surface plasmon, to changes in refractive index. SPR sensors can be classified based on the method for optical excitation of surface plasmons and the measured characteristic of the light wave interacting with the surface plasmon.

SPR sensors directly measure refractive index. In conjunction with appropriate biorecognition elements, they can be used as affinity biosensors allowing detection of the capture of analyte molecules by biorecognition elements immobilized on the sensor surface. The ability of SPR sensors to perform measurements is described by the performance characteristics, of which the most important are the sensitivity, resolution, accuracy, reproducibility, and limit of detection. The sensitivity and resolution are primarily determined by the properties of the optical system of the SPR sensor and can be linked to specific design parameters.

References

1. Homola J (2006) Electromagnetic Theory of Surface Plasmons. In: Homola J (ed) Surface Plasmon Resonance Based Sensors. Springer Ser Chem Sens Biosens, vol 4. Springer, Berlin Heidelberg New York (in this volume)
2. Homola J (2003) Anal Bioanal Chem 377:528
3. Matsubara K, Kawata S, Minami S (1988) Appl Spect 42:1375
4. Zhang LM, Uttamchandan D (1988) Electron Lett 24:1469
5. Nylander C, Liedberg B, Lind T (1982) Sensor Actuator 3:79
6. Brockman JM, Nelson BP, Corn RM (2000) Ann Rev Phys Chem 51:41
7. Kruchinin AA, Vlasov YG (1996) Sensor Actuator B Chem 30:77
8. Ho C, Robinson A, Miller D, Davis M (2005) Sensors 5:4
9. Tumolo T, Angnes L, Baptista MS (2004) Anal Biochem 333:273
10. de Feijter JA, Benjamins J, Veer FA (1978) Biopolymers 17:1759
11. Thomsen V, Schatzlein D, Mercuro D (2003) Spectroscopy 18:112
12. Currie LA (1997) Chemomet Intel Lab Sys 37:151
13. Homola J, Koudela I, Yee SS (1999) Sensor Actuator B Chem 54:16
14. Nenninger GG, Tobiška P, Homola J, Yee SS (2001) Sensor Actuator B Chem 74:145
15. Johansen K, Arwin H, Lundstrom I, Liedberg B (2000) Rev Sci Inst 71:3530
16. Yeatman EM (1996) Biosens Bioelectron 11:635
17. Drake AW (1967) Fundamentals of applied probability theory. McGraw-Hill, New York
18. O'Brien MJ, Perez-Luna VH, Brueck SRJ, Lopez GP (2001) Biosens Bioelectron 16:97
19. Kawazumi H, Gobi KV, Ogino K, Maeda H, Miura N (2005) Sensor Actuator B Chem 108:791
20. Piliarik M, Vaisocherová H, Homola J (2005) Biosens Bioelectron 20:2104
21. Berger CEH, Beumer TAM, Kooyman RPH, Greve J (1998) Anal Chem 70:703
22. Fu E, Chinowsky T, Foley J, Weinstein J, Yager P (2004) Rev Sci Inst 75:2300
23. Kukanskis K, Elkind J, Melendez J, Murphy T, Miller G, Garner H (1999) Anal Biochem 274:7
24. Goddard NJ, Pollardknight D, Maule CH (1994) Analyst 119:583
25. Sjölander S, Urbanitzky C (1991) Anal Chem 63:2338
26. Stenberg E, Persson B, Roos H, Urbaniczky C (1991) J Colloid Interface Sci 143:513
27. Chinowsky TM, Jung LS, Yee SS (1999) Sensor Actuator B Chem 54:89
28. Tobiška P, Homola J (2005) Sensor Actuator B Chem 107:162
29. Nenninger GG, Piliarik M, Homola J (2002) Meas Sci Technol 13:2038
30. Thirstrup C, Zong W, Borre M, Neff H, Pedersen HC, Holzhueter G (2004) Sensor Actuator B Chem 100:298
31. Dostálek J, Homola J, Miler M (2005) Sensor Actuator B Chem 107:154